11th World Congress on Computational Mechanics (WCCM XI)
5th European Conference on Computational Mechanics (ECCM V)
6th European Conference on Computational Fluid Dynamics (ECFD VI)
E. Oñate, J. Oliver and A. Huerta (Eds)

NON-OSCILLATORY FEM FOR FLOWS OVER FLOODING AREAS AND PARTIALLY ERODIBLE BEDS

PABLO ORTIZ†, JOSÉ GÓMEZ† and JAVIER ANGUITA†

† University of Granada, Esc. Ing. Caminos, Campus Fuentenueva, 18071 Granada, Spain.
e-mail: portiz@ugr.es
correo@josegomez.net
jtokminero@gmail.com

Key words: Evolutionary coastlines, Coupled erodible beds, Positive algorithm, Continuous finite element method.

Abstract. The paper introduces a positive continuous finite element method (FEM) for coupled transport equations, incorporating the shallow water equations and a sediment transport equation. Transport equation relates position of the bed–fluid interface to the divergence of sediment fluxes. The equation is casted as a standard advection–diffusion PDE suitable for an efficient positive–definite continuous FEM model.

The continuous FEM is developed by integrating a high order finite element procedure with a conservative flux–correction that imposes sign–preservation, permitting simulation of flows with dry fronts without spurious mass exchanges and oscillations, as well as simulation of the evolution of layers of erodible sediment over partially non–erodible stratums. Experiments focus on applications of the model to the simulation of real river dynamics and evolution of sediment layers with partially non–erodible beds.

1 INTRODUCTION

Flows over flooding areas in estuaries and rivers are often simulated by the shallow water equations. Computational domain for an estuary/river region is partially confined by an artificial boundary connecting the area with coastal regions or with the open sea, requiring special open boundary conditions (e.g. [8]). Rest of the boundary is mostly defined by evolutionary coastlines, particularly when severe flood conditions occur. These coastlines call for a proper numerical algorithm for the dynamics of dry–wet interfaces. Otherwise, when sediment motion is relevant a coupled transport equation is added. Coupled sediment evolution necessitates a sign–preserving method to calculate the thickness of the erodible layer–a positive definite physical property–when natural beds are constituted by erodible and non–erodible materials. As a bonus, sign–preserving property is beneficial to shrink the oscillatory behavior when computed values are near zero [9]. In our case, null total height of water determines the position of the dry–wet interface.

This work presents a sign–preserving and continuous finite element method (FEM) for coupled transport equations, incorporating the shallow water equations [11] and a sediment transport equation interacting with the fluid flow equations by time–dependent sources for momentum. The bedload transport is written as convective fluxes with the effective velocity representing transport rates averaged over the local effective thickness of the erodible stratum. Otherwise, sediment avalanches, acting as a natural slope limiter, are represented as diffusive fluxes with an anisotropic, inhomogeneous diffusion coefficient depending critically on the local slope [10].

The continuous FEM is founded in the flux corrected transport (FCT) concept [9, 11] (for seminal ideas on FCT, see [1, 17, 18]). The resulting numerical scheme preserves global conservation and positivity simultaneously over a domain comprising totally and partially wet elements, without non–physical flows towards or from dry regions. Besides, the procedure does not require a specific approach for partially wet sub–domains and precision to capture the topology of the interfaces lies in an adequate grid resolution.

The fundamental idea of FCT is to correct a conservative and sign–preserving predictor algorithm (typically with large diffusion error) with antidiffusive contributions. These contributions preserve the properties of the predictor scheme, resulting in an enhanced solution with a reduced residual error. The goal is reached by choosing a high order solution such that the correction is calculated by limiting the difference between the contributions of the high order method and those of the predictor method. In this work the high order solution is an approximate second order FEM (see [8] for a thorough formulation).

Numerical experiments concentrates on the evolution of sediment layers over partially non–erodible beds. To simulate bedload transport, two models have been adopted. First, a typical formula for the transport q_s as $q_s \propto u^m$ (see e.g. [16], [14]), where u is the local velocity and m an exponent. Second, formulas of the type of Meyer-Peter-Muller (see e.g. [13]), where wall stress is computed in terms of a depth–integrated friction law.

2 CONTINUOUS AND NUMERICAL MODELS FOR FLOW AND SEDIMENT

2.1 Flow model

Depth–integrated shallow water equations considering an evolutionary bed are

$$\frac{\partial h}{\partial t} + \nabla \cdot (h\mathbf{u}) = 0 \ , \tag{1}$$

$$\frac{\partial (h\mathbf{u})}{\partial t} + \nabla \cdot \mathbf{F} + \nabla p + \mathbf{Q} = 0 \tag{2}$$

in Ω, $t \in [t_0, T]$, with the proper boundary conditions corresponding to the number of ingoing/outgoing characteristic surfaces on the boundary, and initial conditions

$$h(X, t_0) = \overline{h}_0(X)$$

$$\mathbf{u}(X, t_0) = \overline{\mathbf{u}}_0(X) \ \text{ in } \Omega \ , \tag{3}$$

where h is the total height of water, $\mathbf{u}$ is the depth averaged velocity, $\mathbf{F} = h\mathbf{u}\mathbf{u}$, $p = \frac{1}{2}gh^2$ (as a *pressure type* variable), $\mathbf{Q} = \mathbf{Q}(h, \mathbf{U}, X, t)$ is a source term, $(X = (x_l), l = 1, 2)$, Ω is a domain in $\mathbf{R}^2$ bounded by Γ, $\overline{h}_0$ and $\overline{\mathbf{u}}_0$ are specified (the latter a vector) functions (from now on overline designates known values), $\mathbf{U} = h\mathbf{u}$, and $[t_0, T]$ is the time interval.

Source terms are decomposed as $\mathbf{Q}{=}\mathbf{Q}_1(\mathbf{U}, h^n, X, t) + \mathbf{Q}_2(h, X, t)$ in the approximate solution, where superscripts including n indicate time level. By incorporating typical Chezy–Manning friction formula and assuming a parametric dependence on h^n,

$$\mathbf{Q}_1 \approx \max[0, \operatorname{sgn}(h^n - \epsilon)] \ \frac{g\mathbf{U} \parallel \mathbf{U} \parallel}{(Ch^n)^2} \ ,$$

where $g{=}\|\mathbf{g}\|$, $\mathbf{g}$ is the acceleration of gravity, $C{=}R^{1/6}/\mathrm{n}'{\approx}h^{1/6}/\mathrm{n}'$ at $n\Delta t$, n' is the Manning resistant coefficient, R is the hydraulic radius and ϵ is a small number of the order of the unit round-off. If pertinent, this kind of source comprises Coriolis force and wind traction (see [11] for details). Moving beds do not modify the equations after depth–integration (compare Eqs.(1) and (2) with Eqs. (1) and (2) of Ref. [11]), but originates a time–dependent source as

$$\mathbf{Q}_2 = gh\nabla d \ ,$$

where d is the vertical position of the bottom depth. Bottom depth is defined as $d(X, t) = d_s(X) + d^*(X, t)$, where d_s is the upper position of a non–erodible stratum and d^* is the thickness of the erodible sediment layer.

2.2 Sediment transport model

The evolution of the effective sediment layer is governed by the conservation law

$$\frac{\partial d^*}{\partial t} + \nabla \cdot \mathbf{q}_s = \nabla \cdot \mathbf{q}_A, \tag{4}$$

where $\mathbf{q}_s$ is the vertically integrated sediment flux. The flux $\mathbf{q}_A$ represents the avalanche transport as a diffusion flux active if $d^* > 0$,

$$\mathbf{q}_A = -\rho_s \mathcal{K} \nabla d \tag{5}$$

with the diffusion coefficient $\mathcal{K}(\mathbf{x}, t)$ depending critically on the local slope

$$\mathcal{K} \equiv \beta \ \max\big[0, d^*\big] \max\big(0, \operatorname{sgn}(\parallel \nabla d \parallel - s_C)\big) \ , \tag{6}$$

where β is the diffusivity value specified in terms of temporal and spatial resolution of the numerical model [7], s_C is the critical slope (e.g. $s_C \equiv \tan\alpha = 0.625$ for sand, where α is the angle of friction) and $\rho_s = \rho_m(1 - \lambda)$ is the bulk density of the sediment with ρ_m and λ denoting, respectively, density of the grain material and porosity (volume fraction of voids).

Sediment flux $\mathbf{q}_s$ is essentially ascribed to saltation, a process that includes particle-size scale direct momentum transfer from the fluid to the grains and ejection due to grain collisions [15]. A succesful model for saltation transport is Bagnold's formula, adjusted by Lettau and Lettau[4]. In Bagnold's formula $\mathbf{q}_s \propto \mathbf{u}_*\|\mathbf{u}_*\|^2$, where $\mathbf{u}_* \equiv u_*\mathbf{u}\|\mathbf{u}\|^{-1}$, the friction velocity $u_* = \sqrt{\rho^{-1}\tau_w}$, ρ is the fluid density and τ_w denotes the wall shear stress. Realistic Bagnold's formula response depends crucially on a detailed calculation of the wall stress field. In this work we compute bedload sediment transport by two models. First model is customized for Struiksma experiment [16], assuming $\mathbf{q}_s \propto\|\mathbf{u}\|^5$. The well–known Meyer–Peter and Muller (MPM) formula (see e.g. [13]) facilitates computation of wall stress and sediment transport by the usage of depth–integrated procedures, and is then employed as second sediment transport model.

Meyer–Peter and Muller formula can be written as

$$\mathbf{q}_s = 8\rho_s D_m^{3/2} g^{1/2} \tilde{\Delta}^{1/2} \max[0, \tau_n - 0.047]^{3/2} \ . \tag{7}$$

Here, D_m is the average sediment diameter at bottom, $\tilde{\Delta}$=(ρ_m-ρ)/ρ, τ_n is the non–dimensional stress and 0.047 is a non–dimensional threshold stress value. Threshold stress value depends on the local bottom slope [10][7] and hence a constant threshold value is valid for smooth local slope variations. The non–dimensional stress is computed as

$$\tau_n = \Big(\frac{\mathrm{n_m}}{\mathrm{n'}}\Big)^{3/2}\Big(\frac{h\,\mathbf{S}_0}{D_m\,\tilde{\Delta}}\Big)$$

where $\mathrm{n_m}$=$(D_{90})^{1/6}$/26 is the particle roughness, D_{90} is the particle diameter at 90 percent finer than particle diameter, and $\mathbf{S}_0$ is the local bottom slope. To adapt the transport formula to a two–dimensional approach, we assume that resultant sediment flux direction coincides with local velocity direction.

To accommodate conservation law to the solution procedure, we arrange Eq. (4) as an advection–diffusion equation,

$$\frac{\partial d^*}{\partial t} + \nabla \cdot \mathbf{U}_s d^* = -\rho_s \nabla \cdot \mathcal{K} \nabla d \ . \tag{8}$$

The advective velocity $\mathbf{U}_s \equiv \mathbf{q}_s/d^*$ is an average velocity over the potentially mobilized sand layer of thickness d^*. Apart from a small-scale episodic dissipative term on the rhs — de facto combinable into the advective flux — in the asymptotic limit of constant $\mathbf{U}_s$, Eq. (8) implies translation of d^* without change of shape.

2.3 Flow and transport numerical model

To construct the flux corrected methodology, proper high order and low order solutions must be defined. High order numerical solution is attained by the continuous characteristic based split FEM (CBS) [8]. Time discretization is formulated by the characteristic based method–see Appendix A in [9]–while spatial discretization employs standard Galerkin

procedure. CBS method is completed by a suitable variable splitting (see full derivation in Ref. [11]). The low order approach is an upwind monotone scheme independent of the HO procedure [9, 11].

Formulation of flux corrected principles starts by writing the finite element high order solution for Eqs. (1),(2), and (8) in matrix form as

$$\frac{1}{\Delta t}\mathbf{C}\,\Delta\mathbf{B} = \mathbf{R}_H \ , \tag{9}$$

where $\mathbf{C}$ is the left hand side matrix for the model problem (in the case of the discrete form of Eqs. (1) and (8) corresponds to the consistent mass matrix $\mathbf{M}_c$). Next, we include the predictor-type monotonic (or positive definite) solution in matrix form as

$$\frac{1}{\Delta t}\mathbf{M}'_L\Delta\mathbf{b} = \mathbf{R}_L \ , \tag{10}$$

where $\mathbf{M}'_L$ is a conservative diagonal matrix ensuring sign. The right hand sides $\mathbf{R}_H$, $\mathbf{R}_L$ correspond to the high order algorithm and to the predictor algorithm, respectively. In the present solution, forcing is modified by an additional term coming from the evolutionary character of the bottom. $\mathbf{B}$, $\mathbf{b}$ represent the unknown for high order and predictor method, respectively. If Eq. (9) is written as

$$\frac{1}{\Delta t}\mathbf{M}'_L\Delta\mathbf{B} = \mathbf{R}_H + \frac{1}{\Delta t}\left(\mathbf{M}'_L - \mathbf{C}\right)\Delta\mathbf{B} \ , \tag{11}$$

by subtracting Eq. (10) from Eq. (11) we have

$$\frac{1}{\Delta t}\mathbf{M}'_L\left(\mathbf{B}^{n+1} - \mathbf{b}^{n+1}\right) = \mathbf{R}_H - \mathbf{R}_L + \frac{1}{\Delta t}\left(\mathbf{M}'_L - \mathbf{C}\right)\left(\mathbf{B}^{n+1} - \mathbf{B}^{n}\right) \ . \tag{12}$$

High order FEM solution can be written as a convenient identity by replacing original low and high order schemes (Eqs. (10) and (9) respectively) on the right hand side,

$$\mathbf{B}^{n+1} = \mathbf{b}^{n+1} + \sum_{j=1}^{E}(\mathbf{M}'_L)^{-1}\{(\mathbf{M}'_L)_j(\mathbf{B}^{n+1} - \mathbf{b}^{n+1})_j\} \ , \tag{13}$$

where the assembling of the product $(\mathbf{M}'_L)_j(\mathbf{B}^{n+1} - \mathbf{b}^{n+1})_j$ for each j element is explicitly written and extended over the total number of elements. Now, introducing the *element contribution* [5] as

$$\mathbf{A}_j = (\mathbf{M}'_L)^{-1}\{(\mathbf{M}'_L)_j(\mathbf{B}^{n+1} - \mathbf{b}^{n+1})_j\} \ ,$$

the identity (13) for a node i is

$$\mathbf{B}_i^{n+1} = \mathbf{b}_i^{n+1} + \sum_{j=1}^{e}\mathbf{A}_j = \mathbf{b}_i^{n+1} + \sum_{j=1}^{e}(\mathbf{A}_j^H - \mathbf{A}_j^L) \ , \tag{14}$$

where the sum of $\mathbf{A}_j$ extends over e, the total number of elements j surrounding i. The high order solution $\mathbf{B}_i$ at time $(n+1)\Delta t$ results from updating the LO solution at time $(n+1)\Delta t$ by the sum of *anti-diffusive contributions* $\mathbf{A}_j$, that counterbalance the first order truncation error of the low order method. Accordingly, the element contribution is the difference between that obtained by the HO solution $\mathbf{A}^H$, and that obtained by the LO scheme, $\mathbf{A}^L$.

A low order solution $\mathbf{b}'$ could be achieved by adding sufficient diffusion $\mathbf{D}$ to the HO method and considering the lumped mass matrix, as proposed in [5]. This new LO solution can be computed as

$$\frac{1}{\Delta t}\mathbf{M}'_L\Delta\mathbf{b}' = \mathbf{R}_H + \mathbf{D} \ , \tag{15}$$

producing the particular element contribution

$$\mathbf{A}_j = (\mathbf{M}'_L)^{-1}\{(\mathbf{M}'_L - \mathbf{C})\Delta\mathbf{B} - \Delta t\mathbf{D}\}_j \ . \tag{16}$$

When the LO solution is computed by Eq. (15), the identity (13) is fulfilled by the original HO solution.

Equation (14) permits to envisage the natural idea of correction by limiting the element contributions, resembling the original concept of flux correction [1]. Then, we construct an improved solution $\tilde{\mathbf{B}}_i$ as

$$\tilde{\mathbf{B}}_i^{n+1} = \mathbf{b}_i^{n+1} + \sum_{j=1}^{e}\tilde{\mathbf{A}}_j = \mathbf{b}_i^{n+1} + \sum_{j=1}^{e}\mathbf{c}_j\mathbf{A}_j \ , \tag{17}$$

where the $\mathbf{c}_j$'s are elementwise correcting functions depending on nodal HO solution, nodal LO solution and the element contribution to the node of the k variables, while its range is: $0 \leq c_{jk} \leq 1$, $c_{jk} \in \mathbf{c}_j$, and $(k = 1, 3)$ for the shallow water equations.

The original FEM-FCT [5] employs the Taylor-Galerkin finite element method [2] [6] as HO option, while the LO scheme is the same algorithm with lumped mass matrix plus added diffusion of the type $(\mathbf{M}_c - \mathbf{M}_L)\mathbf{B}^n$. The low order method defined by Eq. (15) is of this type and in this case the flux correction is constructed by using the element contribution given by Eq. (16), while solution (17) is conservative. A more general methodology can be devised by including a solution $\mathbf{b}$ independent of the HO scheme. If element contributions are computed by Eq. (16), the identity (13) yields to a modified HO solution $\mathbf{B}'$ given by

$$\mathbf{B}' = \mathbf{B} + (\mathbf{R}_L - \mathbf{R}_H)\Delta t - \Delta t\mathbf{D} \ . \tag{18}$$

The actual range of the corrected solution is between the new LO solution and the modified solution (18). Furthermore, the correction procedure given by Eq. (17) must preserve global conservation. The adding of anti-diffusion of the type of Eq. (16), where $\mathbf{D} \propto (\mathbf{M}_c - \mathbf{M}_L)\mathbf{B}^n$, ensures conservation of the correcting procedure if the LO solution is conservative.

2.4 Flux correction for a coupled set of variables

We construct a basic framework of computation as,

1. Computation of the high order solution **B** (Eq. (9)).
2. Computation of the low order solution, **b** (Eq. (10)).
3. Determination of bounds B^{min}, B^{max} (see [11]).
4. Calculation of the correcting functions by one of the procedures described below.
5. Computation of anti-diffusive contributions and $\tilde{\mathbf{B}}$ (Eq. (17)).

In the case of a coupled set of variables, efficiency of the anti-diffusion technique depends strongly on the selection of the correcting functions. The simple extension of a scalar computation of the corrections [9] for each one of the conservative variables of Eqs. (1) and (2) separately could result in inappropriate constraints for some of the variables. The construction of limiters that synchronize variables has a large degree of empiricism mainly due to its pronounced case-dependent character (see [3] and [5]). Here, we embedded in the solution two simple synchronies. The first strategy, based on that proposed in [5], defines the i nodal values of the correcting function as

$$c_i^+ = \min(c_{ik}^+) \; ; \quad c_i^- = \min(c_{ik}^-) \; ,$$

where $k = 1, 3$ for the set of the conservative variables and, optionally, for the non-conservative variables. The second method limits variables with physically sound constraints. For this purpose, we used the nodal minimum, while now $k = 1, 2$, where $k = 1$ is for the total height h, and $k = 2$ is for the non-conservative specific energy $e = h + \mid \mathbf{u} \mid^2 /2$. In case of the sediment transport equation, an independent computation of limiters is sufficient.

3 NUMERICAL EXPERIMENTS

We present a summary of a complete series of results (to be published) corresponding to two main experiments. The first experiment is the numerical simulation of a laboratory test carried out by Struiksma [16]. The study was performed in a straight flume with an effective length of 11.5 m, a uniform width of 0.2 m, and a vertical brick side wall of 0.5 m. Layers of uniform sand and concrete floor were prepared according to four layouts. In Fig. 1 third arrangement is shown, where bottom level of concrete, representing a non–erodible pile, and initial bottom level of sand is superimposed with experimental and numerical results after 1 h of simulation. A steady discharge (from left to right) of 9.2 l/s is prescribed, while initial mean water depth is h_0=0.106 m. Transport formula and empirical coefficient proposed by Struiksma [16] is $q_s = \alpha u^m$, where α=4.2 and m=5. It is remarkable that, although there is not a threshold condition in the Struiksma's formula,

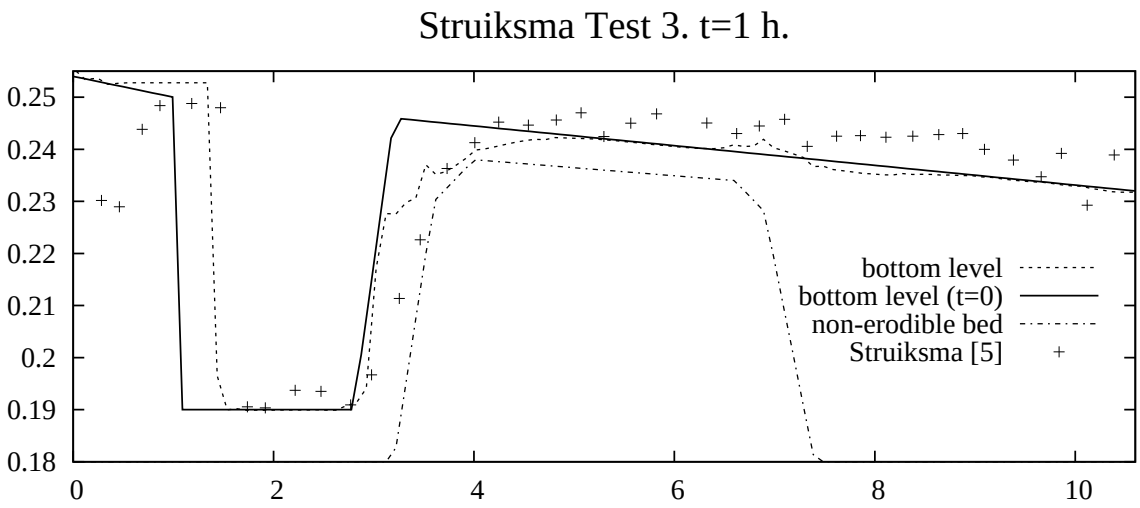

Figure 1 Computed and measured longitudinal bed profiles [16] over a non–erodible bed layer (m) at t=1 h. Initial bed profile and non–erodible pile is superimposed

excess of erosion is not detected in model results. Agreement with experiment is good and sign–preservation is strict.

The second study is in a river region (Huercal–Overa, Spain) having a length of more than 2 km (Fig. 2). Across the river two bridges are located. The corresponding road embankments can be seen in Figs. 2 and 3. In Fig. 2 we represent initial height of water for steady state conditions of flow (210.9 m^3/s), assuming a non–erodible initial bed. Regions with the lower color of the scale (h=0) are dry areas. The triangular mesh has 17594 elements and 8959 nodes; sediment transport model is MPM model described in Section 2.2. Initial conditions for the hydrodynamics is assumed as a steady state reached for non–erodible conditions. Figures 3, 4, and 5 plot bottom levels for 400 s (initial), 476 s, and 514 s, respectively. Evolution shows a substantial deposition in a region downward and close the second embankment.

4 CONCLUSIONS

A method is developed by integrating a high order finite element procedure with a conservative correction that imposes sign–preservation, permitting simulations of flows with dry fronts and with evolutionary sediment bottoms and coastlines without spurious mass exchanges and oscillations. Experiments illustrate the suitability of the model for shallow water equations coupled with sediment transport equations casted as convection–diffusion equation for a non–negative scalar property. In particular, the model is a useful tool to simulate severe flood conditions in large areas, including morphodynamics processes for which bed motion interacts with the flow and with the drying–wetting interface evolution.

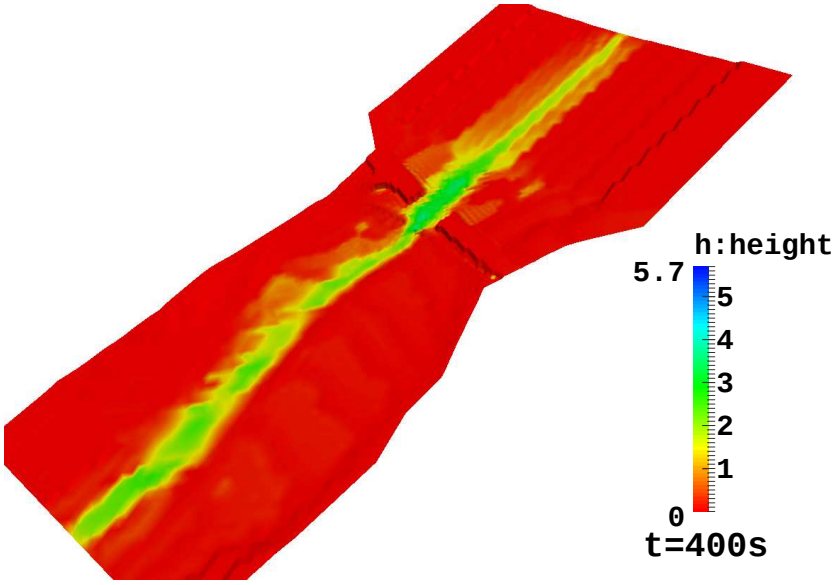

Figure 2 Huercal–Overa. Height of water(m). t=400 s

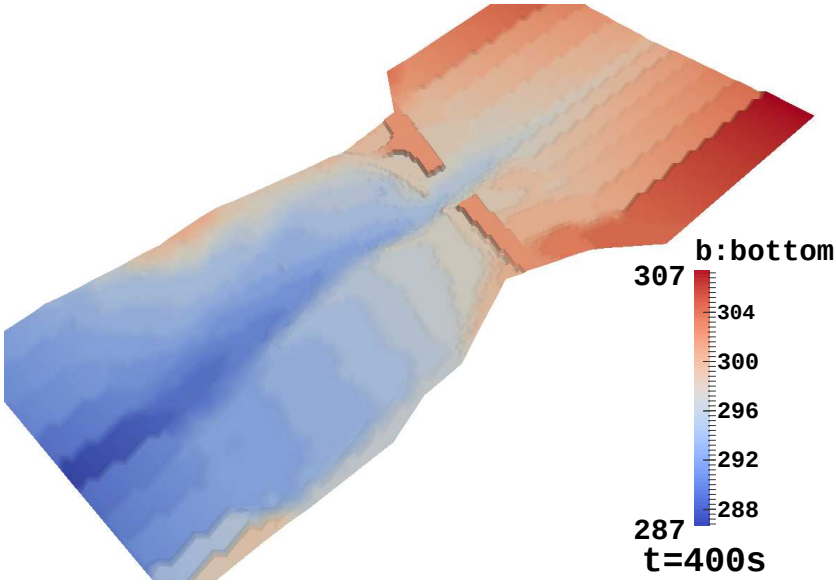

Figure 3 Huercal–Overa. Bottom level(m). t=400 s

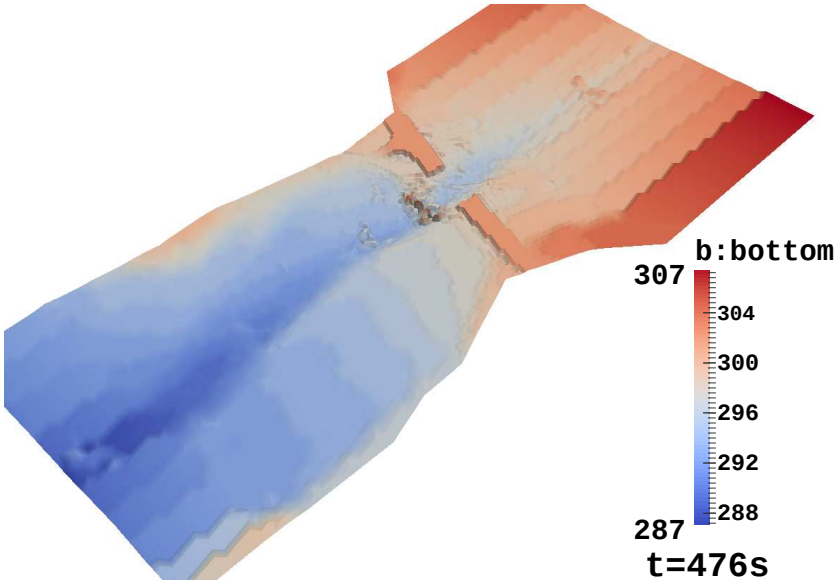

Figure 4 Huercal–Overa. Bottom level(m). t=476 s

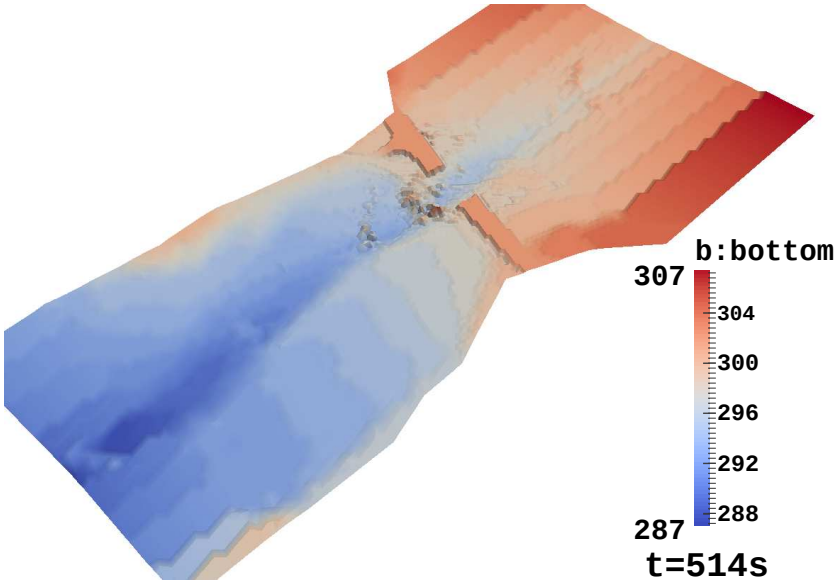

Figure 5 Huercal–Overa. Bottom level(m). t=514 s

ACKNOWLEDGEMENTS

We are grateful to the staff of AOPJA (Agency of Public Works of Andalusia Regional Government) for their commitment and efficiency. Many inspiring discussions with researchers of AOPJA helped to improve the work. This work was partially supported by Programa operativo FEDER de Andalucía (2007-2013), Proyecto: Bases científicas para una guía de cálculo hidráulico de Estructuras de Drenaje en la Red viaria Andaluza (AOPJA-G-GI300/IDI0). First author was also partially sponsored by the MICIIN Grant BIA-2012-32918. Figures 2–5 were plotted using ParaView [12].

REFERENCES

[1] Boris, J.P. and Book, D.L., Flux-Corrected Transport. I. SHASTA, a fluid transport algorithm that works. *J. Comput. Phys.* 1973; **11**, 38-69.

[2] Donea, J., A Taylor Galerkin method for convective transport problems. *Int. J. Numer. Meth. Engng.* 1984; **20**, 101-119.

[3] Kuzmin, D. and Möller, M., Algebraic flux correction II. Compressible Euler Equations. In D. Kuzmin, R. Lohner and S. Turek, Flux Corrected Transport: Principles, Algorithms and Applications, *Springer*, 2005; 208-251.

[4] Lettau, K. and Lettau, H.H., Experimental and micro-meteorological field studies of dune migration, in: H.H Lettau and K. Lettau (Eds.), Exploring the Worlds Driest Climate, Lettau and Lettau, U. of Wisconsin, Madison, 1978.

[5] Lohner, R., Morgan, K., Peraire, J. and Vahdati, M., Finite element flux-corrected transport (FEM-FCT) for the Euler and Navier-Stokes equations. *Int. J. Numer. Meth. Fluids* 1987; **7**, 1093–1109.

[6] Ortiz, P., A Taylor Galerkin implicit explicit generalization for convection diffusion equations. In T.F. Russell et al, Numerical Methods in Water Resources, *Elsevier* Vol. I, 1992; 165–172.

[7] Ortiz, P. and Smolarkiewicz, P.K., Numerical simulation of sand dune evolution in severe winds. *Int. J. Numer. Meth. Fluids* 2006; **50**, 1229–1246.

[8] Ortiz, P., Zienkiewicz, O.C. and Szmelter, J.. Hydrodynamics and transport in estuaries and rivers by the CBS finite element method. *Int. J. Numer. Meth. Engng.* 2006; **66**, 1569–1586.

[9] Ortiz, P., A positive definite continuous FEM model for advection. *Adv. Water Res.* 2009; **32**, 1359–1371.

[10] Ortiz, P. and Smolarkiewicz, P.K., Coupling the dynamics of boundary layers and evolutionary dunes. *Phys. Rev. E* 2009; **79 (4)**, 041307-1–11.

[11] Ortiz, P., Non-oscillatory continuous FEM for transport and shallow water flows. *Comput. Methods Appl. Mech. Engrg.* 2012; **223-224**, 55–69.

[12] ParaView (2012). Open Source Visualization. http://www.paraview.org/

[13] Raudkivi, A.J., *Loose Boundary Hydraulics*. Balkema. 1998

[14] Rulot, F., Dewalds,B.J., Erpicum, S., Archembeau, P. and Pirotton, M., Modelling sediment transport over partially non-erodible bottoms. *Int. J. Numer. Meth. Fluids* 2012; **70**, 186–199.

[15] Sauermann, G., Kroy, K. and Herrmann, H.J., Continuum saltation model for sand dunes. *Phys. Rev. E* 2001; **64**, 031305.

[16] N. Struiksma, *Mathematical modelling of bedload trasnport over non-erodible layers.* IAHR Symposium on River, Coastal and Estuarine Morphodynamics, Genova, 89–98, 1999.

[17] Zalesak, S.T., Fully multidimensional flux-corrected transport algorithms for fluids. *J. Comp. Phys.* 1979; **31**, 335-362.

[18] Zalesak, S.T., The design of flux-corrected transport (FCT) algorithms on structured grids. PhD Dissertation; *George Mason University, USA*, 2005.